Stability and bifurcations of periodically modulated, optically injected laser diodes

M. Nizette and T. Erneux
Université Libre de Bruxelles, Optique Nonlinéaire Théorique, Campus Plaine, Code Postal Interne 231, 1050 Bruxelles, Belgium

A. Gavrielides and V. Kovanis
Nonlinear Optics Center, Air Force Research Laboratory, 3550 Aberdeen Avenue S. E., Kirtland Air Force Base, New Mexico 87117-5776

(Revised Manuscript 06 June 2000; published 24 January 2001)

Recent experiments using lasers subject to external injection [T. B. Simpson, Opt. Commun., **170**, 93 (1999)] have shown remarkable locking performances when a small reference current modulation is added to the dc-bias current. The locking problem is studied analytically by using a multiple scale perturbation method. We derive a slow time amplitude equation for the laser rapid limit-cycle oscillations. The solution of this equation is then investigated both analytically and numerically using a continuation method. We find that the intensity of the laser field can be time periodic (locking) or quasiperiodic (unlocking) and that there exist two distinct bifurcation mechanisms leading to locking. Finally, we compare bifurcation diagrams based on our amplitude equation with diagrams obtained from the laser original equations and find a good quantitative agreement.

DOI: 10.1103/PhysRevE.63.026212 PACS number(s): 05.45.Xt, 42.55.Px, 42.60.Fc, 42.65.Sf

I. INTRODUCTION

Optical generation and transmission of microwave and millimeter waves is an area that has received considerable attention in the last few years. Various novel device configurations using diode lasers have been tested and the generation and transmission of millimeter waves for 25 km in an optical fiber has been successfully realized [1]. Such advances will greatly benefit the mm-wave communications and the wavelength division multiplexing technology. In addition, a number of applications such as optical control of antennas and optical communications require a spectrally pure microwave oscillator with frequencies in tens of GHz that can easily interface with optical systems. Recent developments in this area have been reviewed in [2]. In particular, optically injected semiconductor lasers are promising devices that can produce high quality microwave radiation at high injection rates [3,4].

It is well known that optical injection may destabilize the steady state of the laser and induce a Hopf bifurcation to sustained intensity oscillations. Stable limit cycles are then produced that manifest themselves as sidebands to the main center line in the optical spectra. Of particular interest is the fact that the frequency of the limit-cycle oscillations may vary from the free running laser relaxation frequency (typically a few GHz) to tens of GHz as a function of the injection strength. For large injection rates and slave-master detunings, the relaxation frequency of the system can reach values as high as 50–80 GHz [5].

However, even though the microwave spectra are easily induced in diode lasers under strong external optical injection, the bandwidth of these sidebands can be broad and of the order of a few hundreds of MHz. This is due to the intrinsic spontaneous noise in the slave laser and to the fluctuations in the injected signal strength rate and slave-master detuning. Phase locking to an external modulation signal at a frequency close to the intrinsic frequency of the limit cycle has been proposed as a stabilizing mechanism [6]. The experiments have produced robust phase locking even under a weak external modulation signal. In addition, the bandwidth of the resulting sidebands experiences large gains and narrow linewidth. This motivates a new study of the laser rate equations modeling a periodically modulated optically injected laser diode.

In our recent analysis of these rate equations, we considered the limit of large values of the linewidth enhancement factor and only periodic solutions were constructed analytically [7]. In this paper, we consider arbitrary values of the linewidth enhancement factor but investigate a different limit of the laser equations, which is motivated by the laser parameters. Specifically, we apply the method of multiple scales and determine a slow time amplitude equation for the laser rapid limit-cycle oscillations. Branches of steady state solutions of this equation are obtained analytically and correspond to time-periodic laser intensity oscillations. Branches of periodic solutions are determined numerically by using a continuation method. They correspond to quasiperiodic laser intensity oscillations. Because steady and periodic solutions of our bifurcation equation are quickly obtained, a systematic study of the laser bifurcations in terms of the modulation depth and the injection rate is possible. Combined analytical and numerical studies of slow time amplitude equations for driven nonlinear oscillators remain rare. However, we show in this paper that bifurcations obtained from an amplitude equation compares quite well with bifurcations obtained from the original evolution equations.

The results of our analysis contribute to a richer view of the periodic locking phenomenon. Indeed, depending on the modulation amplitude, the transition to locking may occur either through a homoclinic bifurcation point or through a Torus bifurcation point. In the first case, the amplitude of the limit-cycle oscillations remains almost steady but the phase of the oscillations is strongly pulsating with a period that becomes infinite at locking. This mechanism is similar to the

familiar Adler's mechanism for steady state locking [8,9]. In the second case, both the amplitude and the phase of the limit-cycle oscillations are pulsating but the period does not change as we approach the locking point. This mechanism is equivalent to a Hopf bifurcation transition but now operating on the amplitude and phase of the laser limit-cycle oscillations.

The paper is organized as follows. In Sec. II, we formulate the laser rate equations in dimensionless form and simplify these equations by taking advantage of the small and large parameters appearing in these equations. In Sec. III, we determine an approximation of the solution that leads to a slow time amplitude equation for the laser rapid limit-cycle oscillations. This approximation is strictly valid for small amplitude solutions but we show in Sec. VI that it quantitatively predicts the behavior of the solution of the original laser equations. In Sec. IV, the bifurcation possibilities of our amplitude equation are analyzed and different bifurcation diagrams are shown in Sec. V. In Sec. VI, we compare bifurcation diagrams obtained from the full laser rate equations and that obtained from the slow time amplitude equation. Finally, we discuss in Sec. VII the originality of our mathematical analysis, the two different routes to locking, and the main effect of a nonzero detuning. All mathematical details have been deferred to appendices for clarity.

II. LASER RATE EQUATIONS

Semiconductor lasers are an example of a class B laser system where the equation describing the polarization of the gain medium can be adiabatically eliminated due to the fast intraband carrier relaxation time. This leaves two equations, one for the electric field within the laser cavity and one for the carrier density, to describe the dynamics of a single-mode laser under optical injection [10,11]. In dimensionless form, the equations for the complex intracavity field amplitude E and the carrier density Z are given by [12].

$$\frac{dE}{dt}=(1-ib)ZE+\Lambda\exp(-i\Omega t), \tag{1}$$

$$T\frac{dZ}{dt}=P-Z-(1+2Z)|E|^2, \tag{2}$$

where time t is measured in units of photon lifetime. Λ and Ω are proportional to the amplitude of the injected field and the detuning frequency between the solitary diode laser and the injected signal, respectively. P is the average value of the dimensionless pumping current above threshold. The fixed parameters b and T are the linewidth enhancement factor that measures the degree of amplitude-phase coupling and the ratio of carrier lifetime to photon lifetime, respectively. The relation between these parameters and the original laser parameters such as the optical frequencies and the photon and carrier lifetimes is shown in the Appendix of [12]. All parameters can be determined experimentally by using four-wave mixing techniques [14] (see also the review in [15]). Numerical simulations of these equations lead to an excellent agreement between numerical and experimental spectra [13].

Introducing the current modulation and inserting $E=\mathcal{E}\exp(-i\Omega t)$ into Eqs. (1) and (2), our laser rate equations take the form [7]

$$\frac{d\mathcal{E}}{dt}=(1-ib)Z\mathcal{E}+i\Omega\mathcal{E}+\Lambda, \tag{3}$$

$$T\frac{dZ}{dt}=P[1+\delta\cos(\omega_m t)]-Z-(1+2Z)|\mathcal{E}|^2, \tag{4}$$

where δ and ω_m are proportional to the amplitude and the frequency of the current modulation, respectively.

In the absence of modulations, the steady state solutions and the stability boundaries are available analytically [16]. The conditions for a Hopf bifurcation point are given in Appendix A. Resonance between the modulation oscillations and the Hopf bifurcation oscillations is possible if

$$P=P_0 \quad \text{and} \quad \Lambda=\Lambda_0, \tag{5}$$

where P_0 and Λ_0 satisfy Eqs. (A2) and (A3) with $\omega_H=\omega_m$. If $\Omega=0$, their leading approximations for T large are given by

$$P_0\simeq P_{00}\equiv\frac{T\omega_m^2}{b^2+1} \quad \text{and} \quad \Lambda_0\simeq\Lambda_{00}\equiv P_{00}\sqrt{(b^2-1)/T}. \tag{6}$$

These expressions will be useful for the nonlinear analysis. In [7], we modeled the experiments by Simpson [6] by considering the following values of the fixed parameters:

$$\Omega=0, \quad T=155, \quad b=5, \quad P=0.25, \quad \omega_m=0.1895. \tag{7}$$

Using the expression of P_{00} in Eq. (6), we find $P_{00}\simeq 0.21$, which is close to the actual value of $P=0.25$. This means that the injected laser operates under nearly resonance conditions. As we shall demonstrate these conditions may have a dramatic effect on the laser bifurcations allowing multiple periodic or quasiperiodic solutions to appear. This motivates a new analysis of the laser equations assuming now (P,Λ) near (P_0,Λ_0). Specifically, we shall apply the method of multiple scales [17,18] and construct a small amplitude time-periodic solution of Eqs. (3) and (4) [19,20]. The long time solution is then described by a slow time amplitude equation that we analyze both analytically and numerically. Steady and time-periodic solutions correspond to periodic or quasi-periodic solutions of the laser original equations. The main objective of this paper is to determine analytically where they appear in the parameter space (Λ,δ). To this end, we shall consider the simplest case of zero detuning $\Omega=0$ and further simplify our laser equations by taking advantage of the relatively large value of T. This is achieved by first introducing the new variables F, z, and s defined by

$$\mathcal{E}\equiv\sqrt{P_0}F, \quad Z=\sqrt{P_0/T}z, \quad s\equiv\omega_m t. \tag{8}$$

Inserting Eq. (8) into Eqs. (3) and (4) and evaluating the resulting equations at $\mathcal{E}=T^{-1}=0$ leads to the following problem for F and z:

$$\sigma \frac{dF}{ds} = (1-ib)zF + \beta \frac{\Lambda}{\Lambda_{00}}, \tag{9}$$

$$\sigma \frac{dz}{ds} = \frac{P}{P_{00}}[1+\delta\cos(s)] - |F|^2, \tag{10}$$

where P_{00}, Λ_{00} are defined in Eq. (6) and the coefficients β, σ are defined by

$$\beta \equiv \sqrt{b^2-1} \quad \text{and} \quad \sigma \equiv \sqrt{b^2+1}. \tag{11}$$

Equations (9) and (10) are now in a form appropriate for a bifurcation analysis. The case T large but fixed has been examined numerically but we have found no qualitative differences with the limiting case $T^{-1}=0$. Furthermore, the important case $|\Omega| \neq 0$ has also been investigated by the multiple scale method and the main differences with the zero detuning case will be described elsewhere.

III. SLOW TIME AMPLITUDE EQUATION

In this section, we determine a small amplitude solution of Eqs. (9) and (10). If $\delta=0$, $P=P_{00}$, and $\Lambda=\Lambda_{00}$, the linearized equations for the steady state admit a 2π-periodic solution with an arbitrary amplitude. Our goal is to determine an equation for this amplitude assuming δ small, P slightly higher than P_{00}, and Λ close to Λ_{00}. To this end, we introduce a small parameter ν defined by

$$P \equiv P_0(1+\nu^2) \tag{12}$$

and expand the other parameters Λ and δ as

$$\Lambda = \Lambda_0(1+\nu^2\lambda), \tag{13}$$

$$\delta = \frac{P_0}{P}\nu^3\Delta \simeq \nu^3\Delta, \tag{14}$$

where λ and Δ are $O(1)$ quantities. The factor P_0/P in Eq. (14) has been introduced in the expansion of δ for algebraic convenience only. Note from Eqs. (12) and (13) that we consider values of (P,Λ) near the exact point of resonance (P_0,Λ_0) instead of its leading approximation (P_{00},Λ_{00}). This particular choice does not affect the perturbation analysis but allow a better quantitative comparison between bifurcation diagrams based on our approximation and bifurcation diagrams obtained numerically from the laser rate equations.

We now seek a solution in power series of ν and apply solvability conditions. The perturbation analysis is long and tedious (see Appendix B) but lead to a series of relatively simple analytical results. The leading approximation of the intensity of the laser field is given by

$$|\mathcal{E}|^2 = P[1+\nu\sqrt{2}|A|\cos(\omega_m s+\phi)+O(\nu^2)], \tag{15}$$

where $A=|A|\exp(i\phi)$ satisfies the following amplitude equation:

$$c_1\frac{dA}{d\tau} = b\Delta + A(c_2+c_3\lambda+c_4|A|^2). \tag{16}$$

In Eq. (16), $\tau \equiv \nu^2 s$ is defined as a slow time variable and $c_1 \ldots, c_4$ are constant coefficients given by

$$c_1 = 2(\beta^2 - 2i\beta + 2), \tag{17}$$

$$c_2 = -i(\beta^2 + 2i\beta - 2), \tag{18}$$

$$c_3 = 2i\beta^2, \tag{19}$$

$$c_4 = \frac{i(\beta^4 + i\beta^3 + 2\beta^2 + 4i\beta - \frac{4}{3})}{(2+i\beta)(1-i\beta)}, \tag{20}$$

where $\beta=\beta(b)$ is defined by Eq. (11). Equation (16) is the main mathematical result of this paper. In the next section, we analyze its solutions in terms of the bifurcation parameter λ and for fixed values of b and Δ.

IV. PHASE-LOCKED SOLUTIONS

Periodic, phase-locked solutions of the original system (3) and (4) correspond to solutions of Eq. (16) that are constant in phase and modulus. Setting $dA/d\tau=0$ in Eq. (16) yields an equation for $A=A_0$, which is given by

$$b\Delta = -A_0(c_2+c_3\lambda+c_4|A_0|^2). \tag{21}$$

Taking the square of the modulus of both sides, we obtain a cubic equation for $|A_0|^2$ of the form

$$b^2\Delta^2 = |A_0|^2|c_2+c_3\lambda+c_4|A_0|^2|^2. \tag{22}$$

We wish to determine the stability properties of the phase-locked solution $A=A_0$. After substituting $A=A_0+a$ and $A^*=A_0^*+a^*$ into Eq. (16) and its complex conjugate, we formulate the linearized equations for a and a^*. We then determine the following characteristic equation for the growth rate Γ:

$$|c_1|^2\Gamma^2 - \Gamma[c_1^*(c_2+c_3\lambda+2c_4|A_0|^2)+\text{c.c.}] + |c_2+c_3\lambda + 2c_4|A_0|^2|^2 - |c_4|^2|A_0|^4 = 0, \tag{23}$$

where c.c. means complex conjugate. Note that the characteristic equation does not depend on the phase of A_0. The condition for a steady limit point is obtained by setting $\Gamma=0$ in Eq. (23) and is given by

$$|c_2+c_3\lambda+2c_4|A_0|^2|^2 - |c_4|^2|A_0|^4 = 0. \tag{24}$$

From Eq. (24), we obtain $\lambda=\lambda(|A_0|^2)$ and then from Eq. (22), we determine $\Delta=\Delta(|A_0|^2)$. With this parametric solution, we determine the limit point lines in the (λ, Δ) parameter space. These points limit the domains of limit-cycle solutions of the original laser equations.

A Hopf bifurcation is also possible. We determine the Hopf conditions by introducing $\Gamma=i\omega$ into Eq. (23). From the real and imaginary parts, we obtain

$$c_1^*(c_2+c_3\lambda+2c_4|A_0|^2)+\text{c.c.}=0, \tag{25}$$

$$|c_1|^2\omega^2 = |c_2+c_3\lambda+2c_4|A_0|^2|^2 - |c_4|^2|A_0|^4 > 0. \tag{26}$$

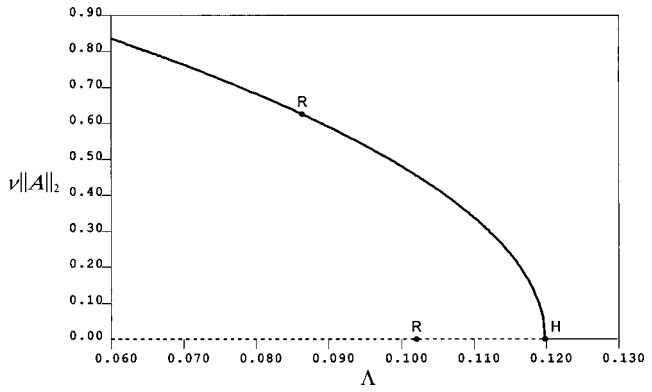

FIG. 1. Bifurcation diagram of the limit-cycle oscillations in the case of no modulation ($\delta=0$). The figure represents the L_2 norm of νA where A satisfies Eq. (16) with $\Delta=0$. The basic steady state solution changes stability at a Hopf bifurcation point labeled by H. The two points denoted by R correspond to points of resonance. The upper point R indicates the value of Λ where the limit-cycle frequency equals ω_m. The lower point R indicates the value of Λ where a small perturbation of the steady state grows with $2\pi/\omega_m$-periodic oscillations. Full and dashed thin lines mean stable and unstable limit-cycle solutions, respectively. The full thick lines represent stable branches of tori.

A Hopf bifurcation corresponds to a Torus bifurcation of the original laser equations. The bifurcation leads to quasiperiodic oscillations exhibiting the two frequencies $\sigma_1=1$ and $\sigma_2=\nu^2\omega$. Using Eqs. (25) and (22), we may again formulate useful implicit expressions for the Hopf bifurcation lines.

In summary, Eqs. (22), (24), and (25) provide analytical stability boundaries that can be analyzed in terms of λ and Δ for different values of b. We have found that the stability diagram shows the same qualitative features for all $b>b_0\simeq 3.872$. In this paper, we shall concentrate on the case $b>b_0$ and describe the possible bifurcation diagrams in detail.

V. BIFURCATION DIAGRAMS

In this section, we determine the bifurcation diagram of the steady and time-periodic solutions of Eq. (16) using the numerical continuation package AUTO [22]. Recall that steady and time-periodic solutions of Eq. (16) correspond to periodic and quasiperiodic solutions of the laser rate equations, respectively.

As in [7], we consider the optical injection rate λ as our control parameter and examine the bifurcation diagram for different values of the pump modulation amplitude Δ. All the other parameters are kept fixed and are listed in Eq. (6). Solving Eqs. (A1)–(A4) numerically, we find $P_0\simeq 0.18$ and $\Lambda_0\simeq 0.087$ and then from Eq. (12) with $P=0.25$, we obtain

$$\nu^2\simeq 0.3777. \tag{27}$$

Because we plan to compare bifurcation diagrams obtained from the amplitude equation (16) and from the full laser equations (3) and (4), we show all our diagrams in terms of the original control parameters Λ and δ [Λ and δ are proportional to λ and Δ, respectively, see Eqs. (12)–(14)].

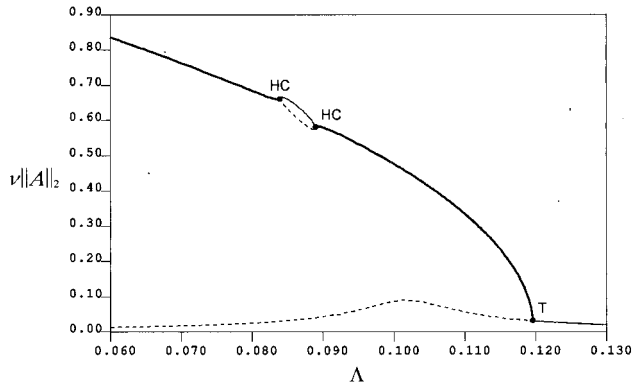

FIG. 2. Bifurcation diagram of the limit-cycle oscillations for low amplitude modulations ($\delta=0.048$). An isola of locked limit-cycle solutions is bounded by the two points HC. It emerges from the upper point R in Fig. 1 as δ is increased from zero. The branch of steady states in Fig. 1 is replaced by a branch of low amplitude oscillations that exhibits a maximum close to the lower point R in Fig. 1. The Hopf bifurcation point H in Fig. 1 becomes a Torus bifurcation point labeled by T. From right to left, the lines emerging from T and finishing at the right HC point and the line starting at the left HC correspond to branches of tori exhibiting quasiperiodic oscillations.

In Figs. 1–5, we show the L_2-norm of νA as a function of Λ for different values of δ. Figure 6 then summarizes the different responses of the laser in the δ versus Λ parameter space. Various symbols label critical points that are described in Table I.

We first examine the case of no modulation ($\delta=0$). See Fig. 1. The basic steady state solution $|A|=0$ transfers its stability to a stable limit-cycle solution as Λ passes below the Hopf bifurcation point $\Lambda_H\simeq 0.12$. If $\delta\neq 0$ but small, the steady state $|A|=0$ is replaced by a branch of $O(\delta)$ periodic oscillations and the Hopf bifurcation point is now a Torus bifurcation point. See Fig. 2. The branch of limit cycles shown in Fig. 1 is now a branch of tori except in an $O(\delta)$ neighborhood of the upper point (R) in Fig. 1. Around this point, we note an isola of limit-cycles locked to the modula-

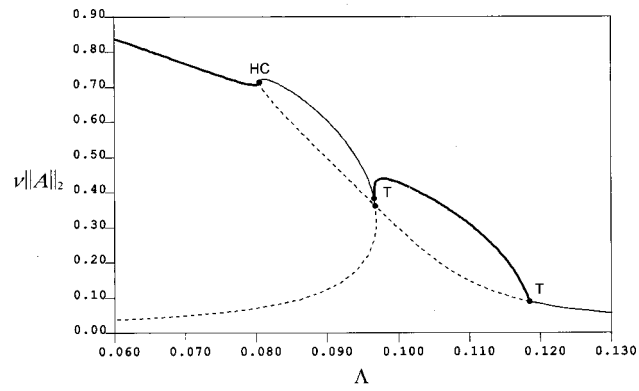

FIG. 3. Bifurcation diagram of the limit-cycle oscillations as two branches of periodic solutions connect ($\delta=\delta_c\simeq 0.1294$). The branch of low amplitude oscillations and the isola in Fig. 2 connect. For δ slightly less than δ_c, the right HC point became a Torus bifurcation point.

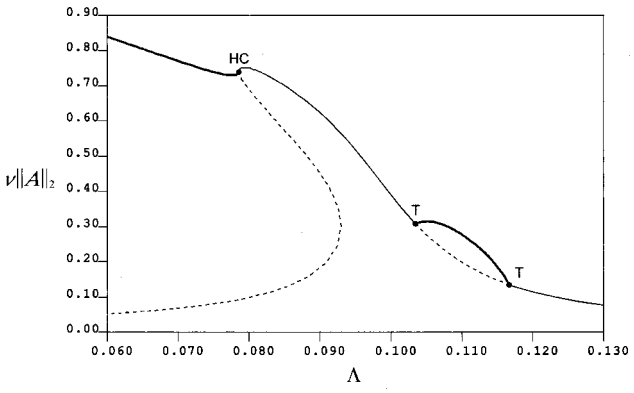

FIG. 4. Bifurcation diagram of the limit-cycle oscillations for moderate amplitude modulations ($\delta=0.18$). For $\delta>\delta_c$, the branch of limit-cycle solutions is S-shaped and the two Torus bifurcations points are closer.

tion frequency ω_m. Outside this isola, the tori exhibit quasi-periodic oscillations with frequency ω_m and a new $O(\delta)$ small frequency. This new frequency approaches zero as Λ approaches the points HC. In all our bifurcation diagrams, we have found that the points HC coincide with the LP of the isola although this is not necessarily always the case.

At a critical value of $\delta=\delta_c\simeq 0.1294$, the isola is connecting the branch of low amplitude periodic solutions. See Fig. 3. Note that the right HC point in Fig. 2 has disappeared and that a second Torus bifurcation point has emerged in the bifurcation diagram. This bifurcation appeared at a value of δ slightly below δ_c. For δ slightly larger than δ_c, the two connected branches of limit-cycle solutions unfold and form an S-shaped curve, as illustrated in Fig. 4. Increasing δ further, we note that the two Torus bifurcation points are coming closer, collide, and disappear. Consequently, if δ is sufficiently large, Torus bifurcations are no more possible and the branch of locked limit-cycle solutions is continuous for all Λ as we pass the left HC (see Fig. 5).

Figure 6 summarizes the different responses of the laser in the δ versus Λ parameter space. We have shown that branches of limit cycles and tori may coexist in the bifurcation diagram but bistability is not possible. Increasing or decreasing the injection rate, we observe the same bifurcation diagram. Depending on the modulation amplitude δ, we note three distinct bifurcation diagrams. For low δ (Fig. 2), the oscillations of the intensity lock and unlock through homoclinic bifurcations. This is the same mechanism as Adler's mechanism for steady state locking [8,9]. Indeed, an Adler's equation can be derived from our amplitude equation (16) in the small Δ limit. We do not reproduce this analysis here (see [20] for a similar exercise on a driven oscillator problem). For moderate values of δ (Fig. 4), the oscillations may lock through either a homoclinic bifurcation or through Torus bifurcations. For large values of δ (Fig. 5), Torus bifurcations are no more possible and locking is possible only through a homoclinic bifurcation.

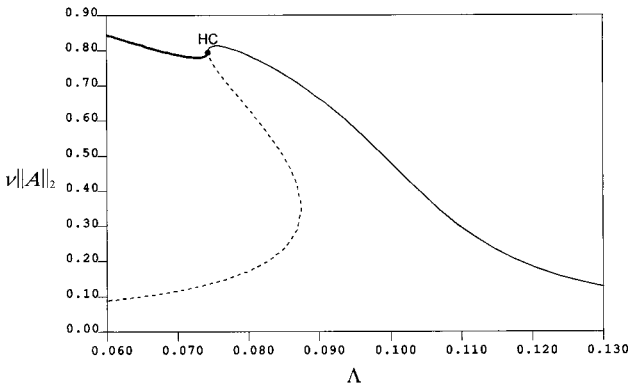

FIG. 5. Bifurcation diagram of the limit-cycle oscillations for high amplitude modulations ($\delta=0.30$). The Torus bifurcation points have merged and have disappeared. As a result, the branch of stable locked solutions is now continuous for all $\Lambda>\Lambda_{\mathrm{HC}}$.

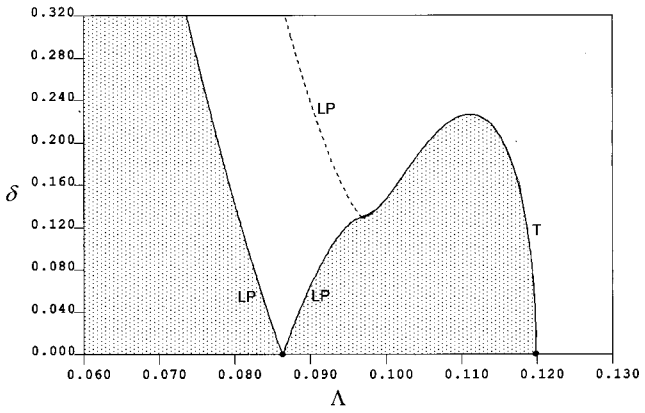

FIG. 6. Possible solutions in the δ versus Λ diagram. Full and dashed LP lines correspond to stable and unstable limit points, respectively. Gray regions limit the regions of unlocked behaviors. For δ smaller than the point connecting the right LP curve and the T curve, the laser locks and unlocks through HC bifurcations that coincide with the LP points. This is the case illustrated by the bifurcation diagram in Fig. 2. For higher values of δ but below the maximum of the T curve, the right LP curve has disappeared. Consequently, the laser locks and unlocks through either a HC point located at the left LP curve or through a Torus bifurcation point. This case is illustrated by the bifurcation diagram in Fig. 4. Above the maximum of the T curve only one locking point appears and is located at the left LP curve. This case is illustrated by the bifurcation diagram of Fig. 5.

VI. QUANTITATIVE COMPARISON OF THE REDUCED AND FULL MODELS

In this section, we compare quantitatively the bifurcation diagrams obtained from the amplitude equation (16) and bifurcations diagrams obtained from solving the full rate equa-

TABLE I. List of the bifurcation and limit points.

H	Hopf bifurcation
T	Torus bifurcation
HC	homoclinic bifurcation
LP	limit point of the limit-cycles

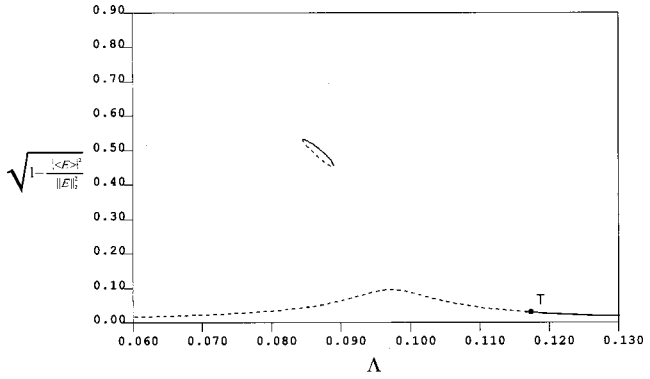

FIG. 7. Numerical bifurcation diagram, the laser limit-cycle oscillations. The solution of the laser equations (3) and (4) is determined for $\delta=0.048$. Stable and unstable periodic solutions have been determined using the continuation method AUTO. Branches of quasiperiodic oscillations cannot be followed. The numerical bifurcation diagram of the periodic solutions compares quantitatively well with the bifurcation diagram of the approximative solutions shown in Fig. 1.

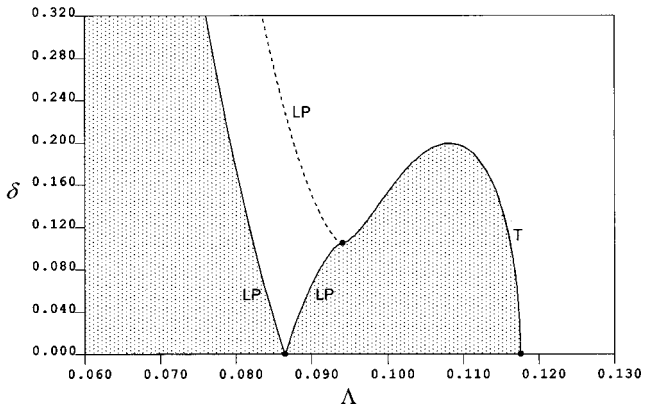

FIG. 8. The domains of periodic solutions in the δ versus Λ diagram. This diagram is determined numerically by finding the periodic solutions of Eqs. (3) and (4). Note that the diagram agrees quantitatively with the analytical-numerical diagram shown in Fig. 6, which is based on solving Eq. (16).

tions (3) and (4). To this end, we again use the continuation package AUTO in order to find the branches of limit-cycle solutions of Eqs. (3) and (4) and determine their stability properties. Note, however, that AUTO is unable to follow branches of quasiperiodic solutions. The agreement between the bifurcation diagrams is excellent. Figure 8 shows the bifurcation diagram obtained for $\delta=0.048$. In this figure, the amplitude of the periodic solutions is determined by computing

$$\mathcal{A}=\sqrt{(\|\mathcal{E}\|_2^2-|\langle\mathcal{E}\rangle|^2)/\|\mathcal{E}\|_2^2} \tag{28}$$

as a function of Λ. $\|\mathcal{E}\|_2^2$ is defined as the squared L_2-norm of the electric field and $\langle\mathcal{E}\rangle$ denotes the time average of the electric field over a period. The expression (28) has a simple physical meaning. Its square represents the ratio of the field power in the sideband modes to the total field power. Using Eq. (15), we find that Eq. (28) clearly matches our analytical expression of the amplitude since

$$\mathcal{A}=\nu|A|+O(\nu^2) \tag{29}$$

as $\nu\rightarrow 0$. The bifurcation diagram shown in Fig. 7 compares quantitatively the bifurcation diagram shown in Fig. 2. Similar comparisons have been done for higher values of δ. The different bifurcation possibilities predicted by solving numerically the laser equations (3) and (4) are shown in the δ versus Λ diagram of Fig. 8. It compares well with the diagram of Fig. 6 based on our asymptotic approximation.

VII. DISCUSSION

The advantages of deriving a slow time amplitude equation for the laser rapid intensity oscillations are twofold. First, we may determine useful analytical expressions for the periodic solutions and their stability boundaries that can be studied in terms of the laser parameters. Second, we are able to use AUTO and follow branches of periodic solutions of the amplitude equation meaning branches of quasiperiodic oscillations of the original laser equations. These branches cannot be determined by AUTO if we directly consider the laser original equations. Surprisingly, the determination of branches of periodic solutions of a slow time amplitude describing a driven oscillator remains rare (see [20,21] for two different problems). We considered the case of zero detuning and used the fact that parameter T is large in order to analyze the simplest form of the laser rate equations. But the method of multiple scales can be applied to the case, T large and fixed. We have found no qualitative changes in the bifurcation possibilities. We also evaluate the validity of our perturbation method by comparing bifurcation diagrams and found a good agreement even if our small parameter that measures the amplitude of the solutions is not very small [from Eq. (27), we find $\nu\simeq 0.6$].

The results of our combined analytical-numerical study of the modulated laser show that there exist two distinct mechanisms for locking. The first mechanism (homoclinic bifurcation) is similar to Adler's mechanism for the steady state locking of the phase of the laser field. Approaching locking, the amplitude of the limit-cycle oscillations remain nearly constant but the phase is pulsating and the period between pulses becomes larger. The second mechanism (Torus bifurcation) is similar to a Hopf bifurcation. Approaching locking, both the amplitude and the phase of the limit-cycle oscillations are oscillating and the frequency changes moderately. These two different routes to locking exhibit different spectra near locking that can be identified experimentally.

In this paper, we considered the case of zero detuning ($\Omega=0$). Our analysis demonstrated that only one stable (periodic or quasiperiodic) solution can be observed as we increase or decrease the injection rate. This is, however, no more the case if $\Omega\neq 0$. A preliminary analysis of this case indicates that two stable regimes may coexist for the same

values of the parameters (bistability) provided that the modulation amplitude is sufficiently large. These predictions are in agreement with recent experiments by Simpson, The detailed analysis of the nonzero detuning case and the experiments will be described in a future publication.

ACKNOWLEDGMENTS

The research of A.G. and V.K. was supported by the U.S. Air Force Office of Scientific Research. The research of T.E. was supported by the U.S. Air Force Office of Scientific Research Grant No. AFOSR F49620-98-1-0400, National Science Foundation Grant No. DMS-9973203, the Fonds National de la Recherche Scientifique (Belgium), and the Inter-University Attraction Pole of the Belgian government.

APPENDIX A: RESONANCE CONDITIONS

In this appendix, we formulate the conditions for resonance between the Hopf bifurcation frequency and the modulation frequency. The Hopf bifurcation conditions are given in [16] for slightly different forms (using $\eta=\Lambda P^{-1/2}$) of the rate equations. We first rewrite the Hopf bifurcation conditions for our Eqs. (3) and (4). The steady state solution $Z=Z(\Lambda)$ is obtained from the implicit expression

$$\Lambda=\sqrt{[(P-Z)/(1+2Z)][Z^2+(\Omega-bZ)^2]}. \tag{A1}$$

Using Z as the bifurcation parameter, the Hopf bifurcation point $Z=Z_H$ satisfies the following equation:

$$(\Omega-bZ)^2Z+\varepsilon b(\Omega-bZ)(P-Z)-\varepsilon(\varepsilon(P-Z)+2Z^2)\times\frac{1+2P}{1+2Z}+Z^3+\varepsilon Z(P-Z)+\varepsilon^2Z\frac{(1+2P)^2}{(1+2Z)^2}=0, \tag{A2}$$

where $\varepsilon\equiv T^{-1}$. The frequency ω_H of the oscillations at the Hopf bifurcation point is then determined from

$$\omega_H^2=-2\varepsilon Z\frac{1+2P}{1+2Z}+2\varepsilon(P-Z)+Z^2+(\Omega-bZ)^2>0. \tag{A3}$$

Resonance at the modulation frequency ω_m is possible if

$$\omega_H=\omega_m. \tag{A4}$$

This condition leads to three equations for $\Lambda=\Lambda_0$, $P=P_0$, and $Z=Z_0$ given by Eqs. (A1), (A2), and (A3), which can be solved numerically.

For $\Omega=0$ and small ε, the high injection Hopf bifurcation point admits the approximation [16]

$$\Lambda_H\simeq P\sqrt{\varepsilon(b^2-1)} \quad \text{and} \quad \omega_H\simeq\sqrt{\varepsilon P(1+b^2)}. \tag{A5}$$

Using (A5), the resonance condition $\omega_H=\omega_m$ gives approximations for $P=P_0$ and $\Lambda_H=\Lambda_0$ as

$$P_0\simeq P_{00}\equiv\frac{\omega_m^2}{\varepsilon(1+b^2)} \quad \text{and} \quad \Lambda_0\simeq\Lambda_{00}\equiv P_{00}\sqrt{\varepsilon(b^2-1)}. \tag{A6}$$

APPENDIX B: PERTURBATION SOLUTION

In this appendix, we determine a solution of Eqs. (9) and (10) by a multiple scale perturbation method. We may decompose the complex field F in amplitude and phase variables but we found more advantageous to work with the variable F and its complex conjugate F^*. All our analysis has been repeated using the symbolic calculus software MAPLE. From Eqs. (9) and (10), we determine equations for F, F^*, and z given by

$$\sigma\frac{dF}{ds}=(1-ib)zF+\beta\frac{\Lambda}{\Lambda_{00}}, \tag{B1}$$

$$\sigma\frac{dF^*}{ds}=(1+ib)zF^*+\beta\frac{\Lambda}{\Lambda_{00}}, \tag{B2}$$

$$\sigma\frac{dz}{ds}=\frac{P}{P_{00}}(1+\delta\cos s)-FF^*. \tag{B3}$$

After inserting Eqs. (12)–(14) into Eqs. (B1)–(B3), we seek a 2π-periodic solution in s of the form

$$F=F_0+\nu F_1(s,\tau)+\nu^2F_2(s,\tau)+\cdots, \tag{B4}$$

$$F^*=F_0^*+\nu F_1^*(s,\tau)+\nu^2F_2^*(s,\tau)+\cdots, \tag{B5}$$

$$z=z_0+\nu z_1(s,\tau)+\nu^2z_2(s,\tau)+\cdots, \tag{B6}$$

where

$$\tau\equiv\nu^2s \tag{B7}$$

is defined as a slow time variable. F_0 and z_0 correspond to the stable steady state solution evaluated at $P=P_{00}$, $\delta=0$, and $\Lambda=\Lambda_{00}$ given by

$$F_0=\frac{1+ib}{\sigma} \quad \text{and} \quad z_0=-\frac{\beta}{\sigma}. \tag{B8}$$

The assumption of two independent time variables requires the chain rule

$$\frac{d}{ds}=\frac{\partial}{\partial s}+\nu^2\frac{\partial}{\partial\tau}. \tag{B9}$$

Introducing Eqs. (B4)–(B6) and (B9) into Eqs. (B1)–(B3) and equating to zero, the coefficients of each power of ν leads to a series of linear problems for the unknown functions $F_1,F_2,\ldots$; $z_1,z_2,\ldots$. We analyze each problem sequentially.

1. $O(\nu)$ problem

The $O(\nu)$ problem is the system (B1)–(B3) linearized around the steady solution

$$\sigma\frac{dF_1}{ds}-(1-ib)(z_0F_1+F_0z_1)=0, \tag{B10}$$

$$\sigma\frac{dF_1^*}{ds}-(1+ib)(z_0F_1^*+F_0^*z_1)=0. \tag{B11}$$

$$\sigma\frac{dz_1}{ds}+F_0F_1^*+F_0^*F_1=0. \tag{B12}$$

Its solution is given by

$$\begin{pmatrix} F_1 \\ F_1^* \\ z_1 \end{pmatrix} = a(\tau)\begin{pmatrix} F_+ \\ F_- \\ 2b \end{pmatrix}\exp(is)+a^*(\tau)\begin{pmatrix} F_-^* \\ F_+^* \\ 2b \end{pmatrix} \times\exp(-is)+\text{edf}, \tag{B13}$$

where a is an unknown complex function of τ, and edf denotes a single exponentially decaying function of s. The constant coefficients $F_\pm$ are defined by

$$F_\pm\equiv\mp(1\pm ib)(1\pm ib+i\beta). \tag{B14}$$

2. $O(\nu^2)$ problem

The solution to the $O(\nu^2)$ problem is given by

$$F_+=F_{2,2}\exp(2is)+F_{2,0}+F_{2,-2}\exp(-2is), \tag{B15}$$

$$F_2^*=F_{2,-2}^*\exp(2is)+F_{2,0}^*+F_{2,2}^*\exp(-2is), \tag{B16}$$

$$z_2=z_{2,2}\exp(2is)+z_{2,0}+z_{2,2}^*\exp(-2is), \tag{B17}$$

where

$$F_{2,2}\equiv\frac{\sigma(1+ib)(\beta+2i)(\beta-i)a^2}{3b^2(b^2+3)} \times\begin{pmatrix}\beta(6ib^2-2b-i)+6ib^3-b^2\\ +2ib-1\end{pmatrix}, \tag{B18}$$

$$F_{2,-2}^*\equiv\frac{\sigma(1-ib)(\beta+2i)(\beta-i)a^2}{3b^2(b^2+3)} \times\begin{pmatrix}\beta(6ib^2+2b-i)-6ib^3-b^2\\ -2ib-1\end{pmatrix}, \tag{B19}$$

$$z_{2,2}\equiv\frac{\sigma(\beta-i)a^2}{3b^2(b^2+3)}[\beta(-13ib^2+i)-3b^4+18b^2+1], \tag{B20}$$

$$F_{2,0}\equiv\frac{1+ib}{\sigma}[\tfrac{1}{2}-2b\sigma^2(b+2i)|a|^2], \tag{B21}$$

$$z_{2,0}\equiv\frac{\beta}{\sigma}[\tfrac{1}{2}-\lambda-2b^2\sigma^2|a|^2]. \tag{B22}$$

3. $O(\nu^3)$ problem

We note that the right-hand side of the $O(\nu^3)$ problem contain terms proportional to the two periodic solutions of the homogeneous problem. This implies that the right-hand side needs to verify a solvability condition. After solving the adjoint linear problem, this condition can be formulated as the integral

$$\int_0^{2\pi}(U_+,U_-,2b) \times\begin{pmatrix} -\sigma\dfrac{dF_1}{d\tau}+(1-ib)(z_1F_2+F_1z_2)\\ -\sigma\dfrac{dF_1^*}{d\tau}+(1+ib)(z_1F_2^*+F_1^*z_2)\\ -\sigma\dfrac{dz_1}{d\tau}-(F_1^*F_2+F_1F_2^*)+\Delta\cos(s)\end{pmatrix} \times\exp(-is)ds=0, \tag{B23}$$

where

$$U_\pm\equiv\pm(1\pm ib+i\beta). \tag{B24}$$

Substituting the various expressions of $F_1,F_2,\ldots$ given above, we obtain from (B23) a differential equation for the complex amplitude a

$$\begin{aligned}4\sigma(\beta^2-2i\beta+2)(1+i\beta)\frac{da}{ds} &= b\Delta-2i\sigma(\beta^2+2i\beta-2)\\ &\times(1+i\beta)a+4i\beta^2\sigma(1+i\beta)\lambda a\\ &+8i\sigma^3\frac{(1+i\beta)^2(\beta^4+i\beta^3+2\beta^2+4i\beta-\frac{4}{3})}{2+i\beta}|a|^2a.\end{aligned} \tag{B25}$$

It can be further simplified by introducing the new variable A defined as

$$A\equiv2\sigma(1+i\beta)a. \tag{B26}$$

In terms of Eq. (B26), Eq. (B25) takes the form of Eq. (16). Moreover, using (B4), the field intensity takes the form of Eq. (15).

[1] Ka-Suen Lee and Chester Shu, IEEE Microwave Guid. Wave Lett. **9**, 192 (1999).
[2] IEEE Trans. Microwave Theory Tech. **45** (8) (1997), special issue on microwave and millimeter-wave photonics.
[3] L. Goldberg, H. F. Taylor, and J. F. Weller, Electron. Lett. **19**, 491 (1983).
[4] X. S. Yao and L. Maleki, Opt. Lett. **21**, 483 (1995).
[5] T. B. Simpson, J. M. Liu, and A. Gavrielides, IEEE J. Quantum Electron. **32**, 1456 (1996); T. B. Simpson and J. M. Liu, IEEE Photonics Technol. Lett. **9**, 1325 (1997).
[6] T. B. Simpson, Opt. Commun. **170**, 93 (1999); T. B. Simpson and F. Doft, IEEE Photonics Technol. Lett. **11**, 1476 (1999).
[7] A. Gavrielides, V. Kovanis, T. Erneux, and M. Nizette, Proc. SPIE **3944**, 627 (2000).
[8] R. Adler, Proc. IRE **34**, 351 (1946) [reprinted in Proc. IEEE **61**, 1380 (1973)].
[9] M. K. S. Yeung and S. H. Strogatz, Phys. Rev. E **58**, 4421 (1998).
[10] G. P. Agrawal and N. K. Dutta, *Long-Wavelength Semiconductor Lasers* (Van Nostrand Reinhold, New York, 1986).
[11] G. H. M. van Tartwijk and D. Lenstra, Quantum Semiclassic. Opt. **7**, 87 (1995).
[12] T. Erneux, A. Gavrielides, V. Kovanis, Quantum Semiclassic. Opt. **9**, 811 (1997).
[13] T. B. Simpson, J. M. Liu, K. F. Huang, and K. Tai, Quantum Semiclassic. Opt. **9**, 765 (1997).
[14] J. M. Liu and T. B. Simpson, IEEE J. Quantum Electron. **30**, 957 (1994).
[15] A. Gavrielides in (unpublished).
[16] A. Gavrielides, V. Kovanis, and T. Erneux, Opt. Commun. **136**, 253 (1997).
[17] J. Kevorkian and J. D. Cole, *Multiple Scale and Singular Perturbation Methods*, Applied Mathematical Sciences Vol. 114 (Springer, New York, 1996).
[18] C. M. Bender and S. A. Orszag, *Advanced Mathematical Methods for Scientists and Engineers* (McGraw-Hill, New York, 1978).
[19] S. Rosenblat and D. S. Cohen, Stud. Appl. Math. **63**, 1 (1980); **64**, 143 (1981).
[20] W. L. Kath, Stud. Appl. Math. **65**, 95 (1981).
[21] S. M. Baer and C. Tier, J. Math. Biol. **23**, 137 (1986).
[22] E. Doedel, T. Fairgrieve, B. Sandstede, A. Champneys, Yu. Kuznetsov, and X. Wang, AUTO 97: Continuation and bifurcation software for ordinary differential equations; http://indy.cs.concordia.ca/auto/main.html.